Modes of active intraplate deformation, Flinders Ranges, Australia

Julien Célérier,[1] Mike Sandiford, David Lundbek Hansen,[2] and Mark Quigley

School of Earth Sciences, University of Melbourne, Melbourne, Victoria, Australia

Received 14 May 2004; revised 12 July 2005; accepted 5 August 2005; published 17 November 2005.

[1] The Flinders Ranges form one of the most seismically active zones within the Australian continent with seismogenic strain rates over the last 30 years of $\sim 10^{-16}$ s^{-1}. Active deformation in the region reflects late Neogene increases in stress levels in the Indo-Australian plate as a response to increased plate boundary forcing from collision zones with the neighboring Asian and Pacific plates. Geological and geophysical observations suggest two modes of active deformation in operation in the Flinders Ranges over the last several million years: (1) low-amplitude ($\sim$200–500 m), long-wavelength ($\sim$200 km) lithospheric flexure and (2) active reverse faulting along the range front with fault slip rates of up to $\sim$50 m Myr^{-1}. Numerical models are developed to explore the contribution of each of these deformation modes to the observed geophysical signals. An elastic mode of deformation is suggested by a distinctive long-wavelength positive correlation between gravity and topography in which the Flinders Ranges are bordered by anomalous topographic and gravity lows, now occupied by playa-lake systems, centered some 50 km outboard of range-bounding faults. Numerical models show that flexural instabilities localized by vertical loads arising from older tectonic structuring produce a first-order match with observed topography and gravity. Numerical models are also used to illustrate how the localized failure evident in the contemporary seismicity and Quaternary faulting record within the Flinders Ranges reflects thermal weakening associated with extraordinary concentrations of heat producing elements in the crust, as reflected in modern-day heat flows of $\sim$90 mW m^{-2}. **Citation:** Célérier, J., M. Sandiford, D. L. Hansen, and M. Quigley (2005), Modes of active intraplate deformation, Flinders Ranges, Australia, *Tectonics*, *24*, TC6006, doi:10.1029/2004TC001679.

1. Introduction

[2] Maps of global seismicity reveal that intraplate earthquakes account for only $\sim$5% of the global seismic moment release, with $\sim$0.5% of the global moment release occurring in so-called stable continental regions (SCRs). However, the often-localized nature of intraplate seismic activity, results in significant seismic moment release in some regions of stable continental regions. For example, in Australia (Figure 1), where the average seismogenic strain rate is less than $\sim 10^{-17}$ s^{-1} [*Johnston*, 1994a], the most active regions are characterized by seismogenic strain rates of $\sim 10^{-16}$ s^{-1} (Figure 2) [*Sandiford et al.*, 2003].

[3] The factors that localize intraplate seismicity have been the subject of considerable debate, with much of the focus on the role of reactivation of zones of prior deformation [*Sykes*, 1978]. Numerous paradigms which aim to further refine *Sykes*' [1978] reactivation hypothesis have been proposed [*Costain et al.*, 1987; *Johnston and Kanter*, 1990; *Sykes*, 1978; *Wesnousky*, 1980], yet little consensus has emerged as to the more specific causes acting to localize and trigger such activity, nor whether ongoing seismicity is associated with other modes of lithospheric deformation. Much of the research on intraplate seismicity in SCRs has focused on the New Madrid Seismic Zone (NMSZ) in the central United States. This region was the site of a sequence of powerful earthquakes in the winter of 1811–1812, for which moment magnitudes of up to M = 8.1 have been estimated [*Johnston and Schweig*, 1996], making them the largest recorded in any intraplate setting. Since the early 1800s the region has continued to be seismically active. Network monitoring in the region began in 1974, and as of that time, 3000 NMSZ earthquakes have been recorded, none of which have reached moment magnitude release of $M \geq 5$ [*Herrmann and Canas*, 1978]. The New Madrid Seismic Zone is hosted within a Late Proterozoic to Early Cambrian failed rift, the Reelfoot rift [*Ervin and McGinnis*, 1975], implying crustal structuring probably plays a crucial role in localizing contemporary seismicity.

[4] For a continent located within a plate interior, Australia shows a surprising level of earthquake activity (Figure 1). Some 7000 earthquakes were recorded in the southeastern portion of Australia in the interval 1958–1999 [*Spassov and Kennett*, 2000]. The most notable of these being the Richter magnitude (M_L) = 5.6 Newcastle earthquake in December 1989, the first since European settlement in which lives were lost. As is observed in other SCRs, seismicity within the Australian continent tends to be a highly localized phenomenon. One of the most active zones is within the Flinders Ranges of South Australia (Figure 3) where the record of neotectonic activity is also particularly well developed [*Sandiford*, 2003]. The relatively high earthquake activity in the Flinders Ranges, combined with the youthful nature of the topography, attest to the role that mild tectonism is playing in shaping the current landscape.

[1] Now at Research School of Earth Sciences, Australian National University, Canberra, Australia.

[2] Now at Department of Earth Sciences, University of Aarhus, Aarhus, Denmark.

0278-7407/05/2004TC001679$12.00

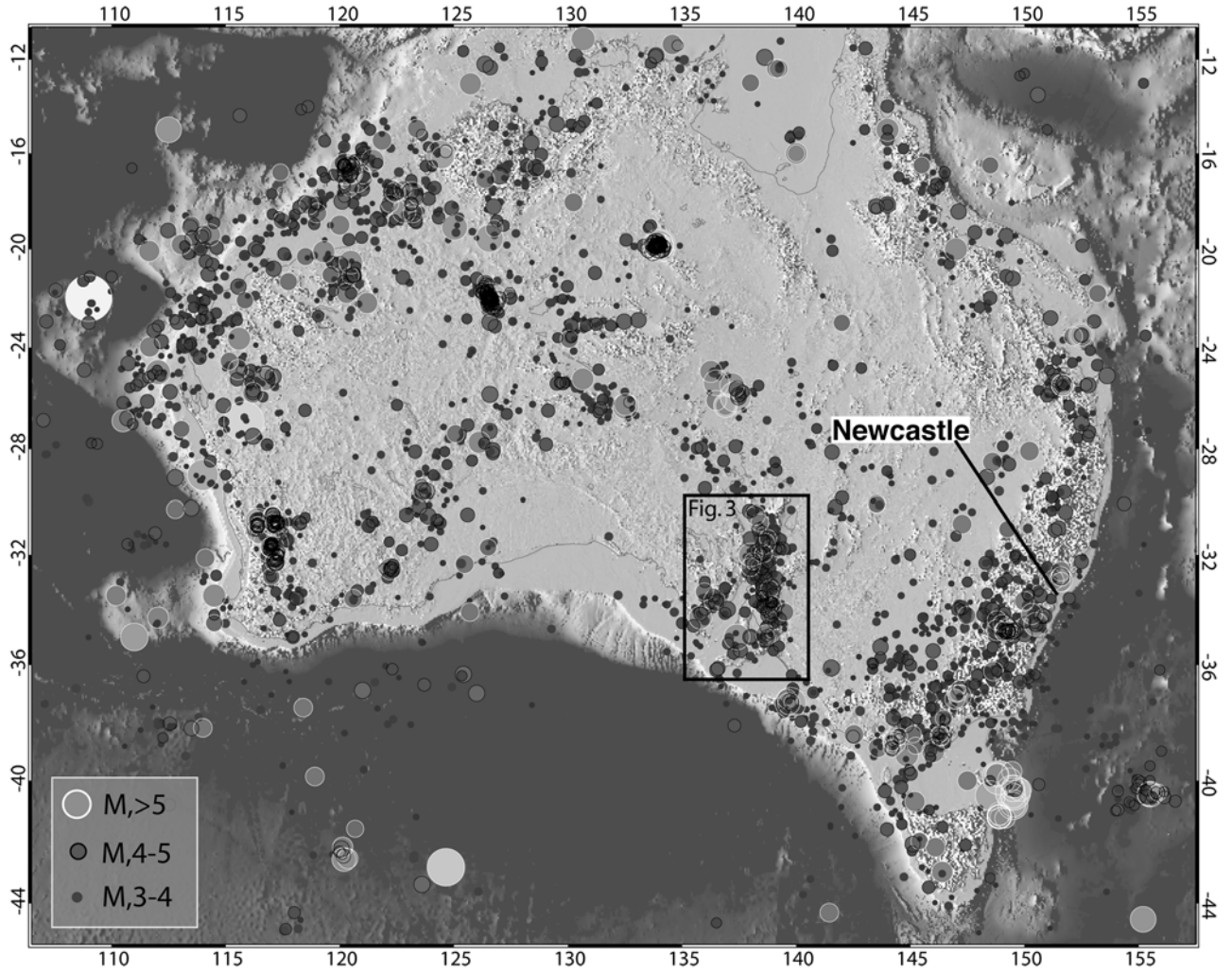

Figure 1. Distribution of Australian seismicity ($M > 3$). Earthquake epicenter data are courtesy of Geoscience Australia. Magnitude measures are based on local magnitudes (M_L) for $M < 5.5$ and surface magnitude (M_s) for $M > 5.5$. See color version of this figure at back of this issue.

[5] Using field based observations and numerical models this paper seeks (1) to compare geologically determined fault slip rates with historical seismic moment release rates, (2) to investigate the factors that localize seismic activity in the region, and (3) to explore the modes of lithospheric deformation that contribute to the geological and geophysical assemblage of the region.

2. Seismicity, Strain, and Stress in South Australia

2.1. Historical and Instrumental Seismicity

[6] In the last 150 years, 15 earthquakes of magnitude 5 or greater have been recorded in South Australia, with between 300 and 400 earthquakes instrumentally recorded each year in the state [*Greenhalgh et al.*, 1994]. The largest instrumentally recorded earthquake in the Flinders Ranges is $M_s \sim 6$, while in southeastern Australia the largest recorded earthquake is $M_s \sim 6.4$. Elsewhere in Australia, $M_s > 6.5$ quakes have occurred at a number of widely distributed localities, with the largest earthquake of magnitude $M_s = 6.8$ (in 1941, near Meeberrie in Western Australia). Most of the contemporary seismicity in South Australia occurs in the Flinders and Mount Lofty Ranges, as well as to a lesser extent along the eastern part of the Eyre Peninsula (Figure 3).

[7] Seismic monitoring in Australia is sufficient for a more or less complete record down to local magnitude (M_L) 3.5 since 1970 [*Gaul et al.*, 1990], allowing estimation of Gutenberg-Richter statistics [*Gutenberg and Richter*, 1944] for earthquake activity rate across the continent (Figure 2). Following *Johnston* [1996], we use the a and b values derived from the Gutenberg-Richter statistics to obtain the seismic moment release rate, M_0:

$$M_0 \approx \frac{1}{\mathrm{t}} \left(\frac{b\left(10^{(a+d)}\right)}{c-b} \right) \left(10^{(c-b)} M_{\max} \right) \tag{1}$$

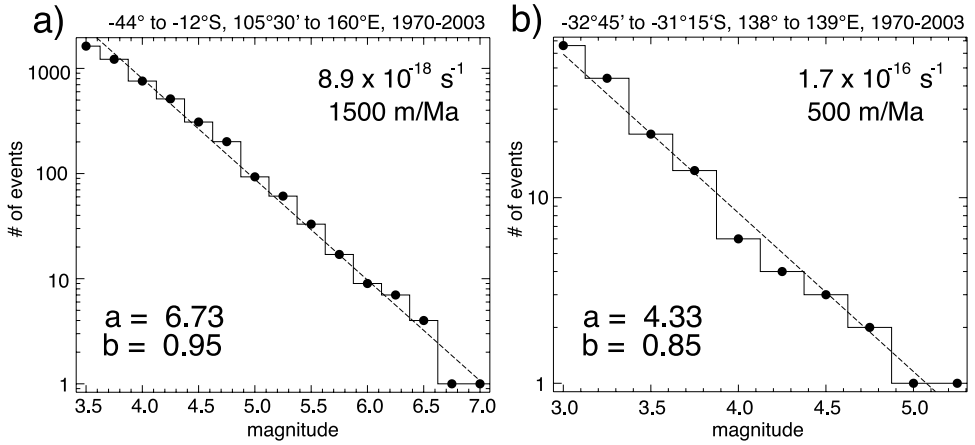

Figure 2. Gutenberg-Richter relations [e.g., *Gutenberg and Richter*, 1944] for the period 1970–2003 and derived seismogenic strain rates for (a) Australian continent and (b) central Flinders Ranges. Seismogenic strain rates and associated shortening rates calculated assuming uniaxial E-W shortening. Note that the Flinders Ranges seismogenic deformation rate is more than 1 order of magnitude higher than the average continental seismicity rate, accounting for approximately one third of the total seismogenic shortening across Australia. Seismogenic strain rate estimates follow the approach of *Johnston* [1994a]. Magnitude measures are based on local magnitudes (M_L) for $M < 5.5$ and surface magnitude (M_s) for $M > 5.5$.

where t is the time span of the seismic record, $M_{\max}$ is the maximum expected magnitude for earthquakes in the region of interest, and c and d are factors that relate to the conversion of magnitude scale to seismic moment [*Hanks and Kanamori*, 1979]:

$$\log(M_0) = c\,M + d \tag{2}$$

In turn, the seismic moment release rate can be used to derive a seismic strain rate [*Kostrov*, 1974]

$$\dot{\varepsilon}_x = \frac{1}{2\mu v} M_0 \tag{3}$$

where μ is the Young's modulus (assumed here to be 8×10^{10} N m^{-2}) and v is the volume of crust in which the seismicity occurs. We assume that the seismogenic zone is 15 km thick, on the basis of the knowledge that the great majority of Australian earthquakes have epicentral depths less than ~10 km [*Gaul et al.*, 1990].

[8] While making these calculations we note that uncertainties in the a and b values, $M_{\max}$, the thickness of the seismogenic zone and the Young's modulus necessarily result in very large uncertainties in estimates of seismic strain rate. Moreover, our poor knowledge of seismic efficiency (i.e., the relative accommodation of strain by seismic and aseismic mechanisms), imply further uncertainty in translating seismically determined strain rates to bulk crustal strain rates [e.g., *Johnston*, 1994b]. Nevertheless, these calculations provide an indication of the sorts of fault slip to be expected if the present-day seismicity is indicative of longer-term geological strain rates.

[9] Since the majority of the moment is carried by the largest, most infrequent, earthquakes, the main uncertainty in the calculation of the seismic strain rates is the value of $M_{\max}$ (Figure 2). For intraplate regions such as Australia with an historical record of only 200 years, it is extremely improbable that this record encompasses an earthquake of magnitude $M_{\max}$. The historical limit therefore provides a lower bound on $M_{\max}$. On longer timescales we would expect somewhat larger earthquakes than those instrumentally recorded, and thus the maximum earthquake expected on geological timescales could conceivably be $M > 7$. Assuming $M_{\max} = 7.0$, the seismic strain rate for the most active region of the Flinders Ranges is $\sim 10^{-16}$ s^{-1} (Figure 2b, see boxed area in Figure 3 for region limits), while the regional background deformation rate, defined in terms of the seismicity of the whole continent, is $\sim 10^{-17}$ s^{-1} (Figure 2a). For example, assuming that the neotectonic deformation record of reverse faulting (see section 3.3) is indicative of essentially uniaxial E-W compression, then a seismic strain rate of $\sim 10^{-16}$ s^{-1} would equate to a shortening rate of several hundred meters per million years across the Flinders Ranges (or ~30% of the total Australian seismic strain). Such a deformation rate could be accounted for an ensemble of 5–10 faults each slipping at ~20–50 m Myr^{-1}. In section 3.3 we outline observations of several range bounding faults that have Quaternary slip rates of this order.

2.2. In Situ Stress Field

[10] The Indo-Australian plate, along with the North American and South American plates, form a group of fast moving continental plates, where the stress fields within the continents is largely "compressional" [*Minster and Jordan*, 1978]. *Cloetingh and Wortel* [1986], *Richardson* [1987], *Coblentz et al.* [1995, 1998] and *Reynolds et al.* [2002] have shown that unlike midplate North America and Western Europe, $S_{H\max}$ in the Australian plate is not aligned parallel

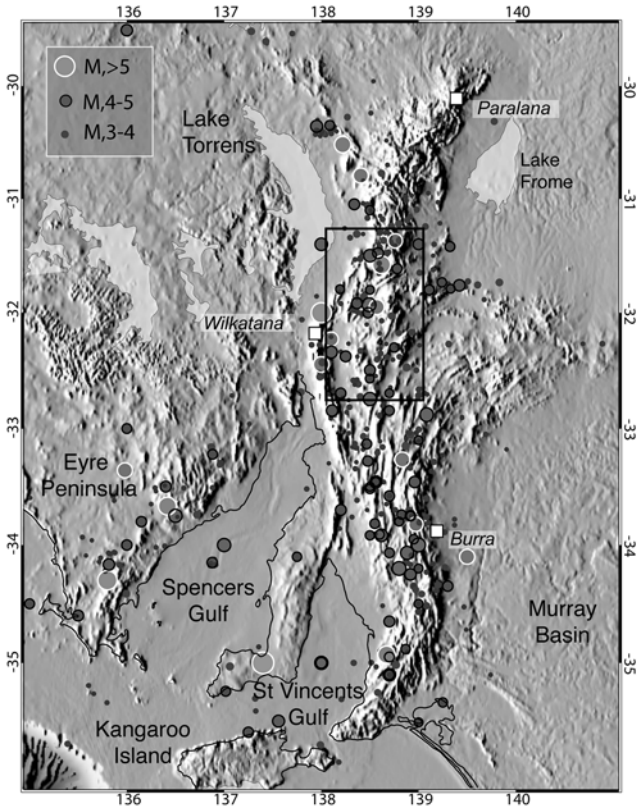

Figure 3. Seismicity pattern of South Australia showing the upland system of the Flinders and Mount Lofty ranges. The Mount Lofty Ranges refer to the southern part of this upland system (south of 34°S), while the Flinders Ranges refer to region north of about 33°30S. Note the anomalously low depressions flanking the ranges (see Figure 4). Around the Flinders Ranges these depressions form internally draining playa lake systems. Earthquake epicenter data are courtesy of Geoscience Australia. Rectangular region shows the region of seismicity used to define Guttenberg-Richter characteristics in Figure 2. Magnitude measures are based on local magnitudes (M_L) for $M < 5.5$ and surface magnitude (M_s) for $M > 5.5$. See color version of this figure at back of this issue.

to the plate motion vector. Rather, in Australia $S_{H\max}$ is oriented E-W in the southwest, E-W to SE-NW in the southeast, NE-SW in the northwest, and NNW-SSW in the northeast [*Coblentz et al.*, 1995].

[11] In the Flinders Ranges, earthquake focal mechanisms show considerable variation in the in situ stress field. Within the northern Flinders Ranges alone, both thrust and strike-slip focal mechanisms are reported, with inferred shortening directions varying between ~020° and ~120°. *Hillis et al.* [1998] attribute this heterogeneity to low horizontal force anisotropy and argue that despite considerable variation in the stress field, there appears to be a poorly defined E-W $S_{H\max}$. In contrast, using a formal inversion of four focal mechanisms, *Clark and Leonard* [2003] have derived a $S_{H\max}$ azimuth of N82°E in a purely strike-slip stress regime, and argue that there is significant horizontal force anisotropy.

[12] *Sandiford et al.* [2004] have related the E-W to SE-NW $S_{H\max}$ trends in southeast Australia to late Neogene changes in the coupling of the Pacific and Australian plates in the late Neogene. *Sandiford et al.* [2004] show that mild compressional tectonics across southeast Australia, as indicated by the modern seismicity, commenced at between 10 and 6 Ma, coinciding with the building of the Southern Alps in New Zealand.

3. Geological Geophysical Framework

[13] Together with the Mount Lofty Ranges, the Flinders Ranges form part of an upland system that extends some 600 km from south of Adelaide to Mount Babbage in the arid continental interior. Here we restrict our discussion to the Flinders Ranges in the region north of latitude 33°30s. The highest peaks in the Flinders Ranges are ~1100 m above sea level. In the northern Flinders Ranges, relief associated with gorges such as Yudnamutana Gorge is locally in excess of 600 m, defining one of the most dramatic and topographically youthful landscapes of the Australian continent. Flanking this upland system are realms of anomalously low topography, with large regions at or below sea level (Figures 3 and 4). The low-lying regions form internally draining, playa lake systems defining a semicontinuous "moat" around much of the northern Flinders Ranges. The playa lakes include Lakes Frome and Callabonna to the east, Blanche, Gregory and Eyre to the north and Torrens to the west (Figure 3).

3.1. Geological Setting

[14] The Flinders Ranges lie almost entirely within the Adelaide Fold Belt, comprising a Paleoproterozoic to Mesoproterozoic cratonic basement overlain by a thick sequence of Neoproterozoic to Cambrian rift sediments [*Paul et al.*, 1999]. This sedimentary package and its underlying crystalline basement were deformed in an orogenic setting in the Late Cambrian–Early Ordovician (~500–490 Ma) Delamerian Orogeny, to form a distinctive oroclinal system now expressed in the strike ridge dominated topography of the Flinders Ranges. Subsequent reactivation during the Devonian and Carboniferous "Alice Springs" events is indicated by a number of low-temperature thermochronometric studies [*Gibson and Stuwe*, 2000; *McLaren et al.*, 2002].

[15] The Paleoproterozoic to Mesoproterozoic crystalline basement of the Flinders Ranges is exposed as variably deformed and metamorphosed, partly fault-bound inliers in the northern Flinders Ranges [*Coats and Blissett*, 1971]. The constituent granites and gneisses of the basement are characterized by extraordinary enrichments in heat producing elements, with heat production rates frequently in excess of 10 μW m^{-3} [*Neumann et al.*, 2000]. Heat flows within the Flinders Ranges average ~90 mW m^{-2}, with a high of 125 mW m^{-2} in the Mount Painter region of the northern Flinders Ranges. The anomalous heat flows form part of a broader region of elevated heat flow extending west-

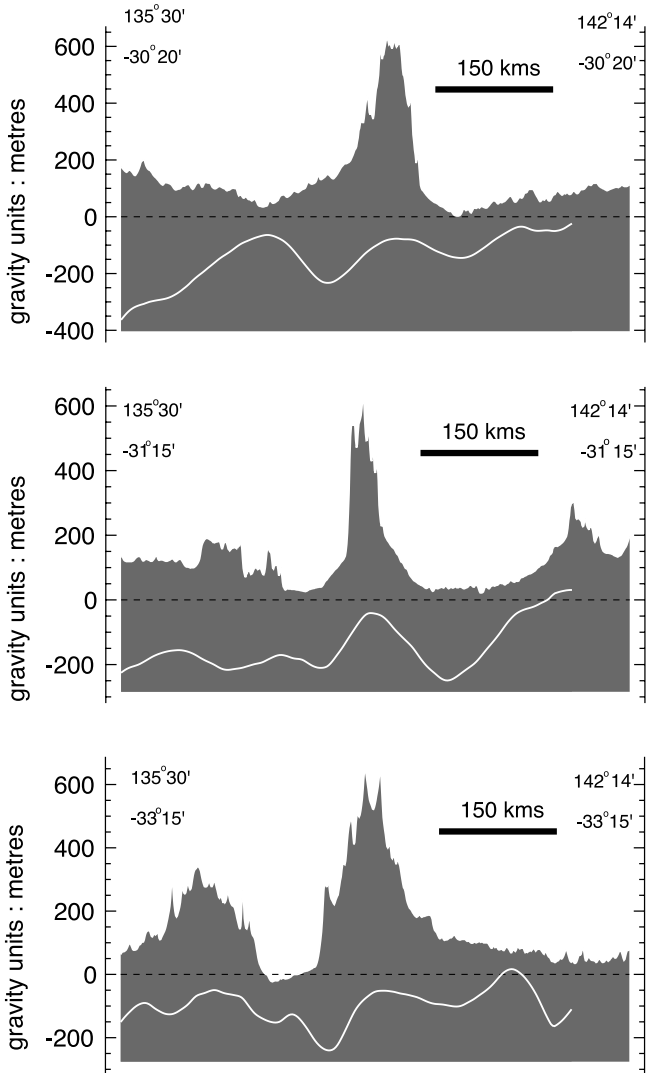

Figure 4. East-west topographic profiles across the Flinders Ranges showing characteristic topographic depressions flanking the ranges, with elevation minima 50–100 km outboard of main range bounding scarps. Elevation data are from AUSLIG 9′ digital elevation model. White curve shows corresponding gravity profile from the MESA (Mines and Energy South Australia) gravity database, measured in gravity units, equal to 0.1 mGal).

ward into the eastern Gawler Craton (average heat flow ~85 mW m^{-2}) and eastward into the Curnamona Craton (average heat flow ~75 mW m^{-2}), values which are typical of much of the Australian Proterozoic crust [*Cull*, 1982; *Houseman et al.*, 1989] and differ from the much lower heat flows of the western Gawler Craton and Archean cratons of Western Australia where heat flows typically lie in the range 35–55 mW m^{-2} [*Cull*, 1982]. *Neumann et al.* [2000] and *McLaren et al.* [2003] show that the high heat flows in the Australian Proterozoic are invariably associated with anomalous heat production in the near surface crust.

[16] Deposited on top of this crystalline basement is a 5–10 km thick Neoproterozoic sedimentary sequence [*Paul et al.*, 1999], understood to have accumulated during an episode of major continental rifting [*Preiss*, 1987]. Sedimentation ceased toward the end of the Cambrian (~520 Ma) with the initiation of a succession of inversion events, associated with the Delamerian Orogeny [*Thomson*, 1969] and the onset of plate convergence along the paleo-Pacific margin. In the Flinders Ranges, both the basement and cover sequences were deformed, with total shortening no more than ~15% [*Paul et al.*, 1999].

[17] Following the Delamerian Orogeny a period of tectonic quiescence ensued with mild thermal perturbations attributed to the late Paleozoic Alice Springs Orogeny [*Gibson and Stuwe*, 2000; *McLaren et al.*, 2002]. During the Mesozoic the region was reduced to a peneplain, after which episodes of fluvial to lacustrine deposition occurred in the Cretaceous, Eocene and Miocene. Intermittent sedimentation in the mid-late Neogene is reflected in low-energy fluviatile and lacustrine sediments of the Namba Formation. On the pediments flanking the northern Flinders Ranges, the Namba Formation is overlain by Pliocene to Quaternary gravels and fanglomerates of the Willawortina and Pooraka formations, indicative of rising topography [*Callen*, 1974].

3.2. Origin of Relief

[18] The origin of the present-day relief of the Flinders Ranges has been the subject of varied opinion. The general lack of recognition of significant young tectonic activity (see discussion in section 3.3) has led most workers to the view that the topography is ancient, extending back at least to the early Cenozoic [*Veevers and Conaghan*, 1984]. In the northern Flinders Ranges, several convincing lines of evidence point to the present-day topography being post-Mesozoic. First, distinctive summit surfaces locally overlain by Cretaceous fluvial sequences imply the present-day relief has been generated since the Mesozoic. Second, range-bounding alluvial fan sequences (Willawortina Formation) seem to have developed only in the late Neogene [*Belperio*, 1995] with older late Miocene sequences (Namba Formation) reflecting low-energy, paralic conditions in the regions bordering the present ranges. *Callen and Tedford* [1976] argued that the transition from low-energy sediments of the Namba Formation to the alluvial fans of the Willawortina Formation in the late Miocene or Pliocene reflects the initiation of uplift of the Flinders Ranges. In recent times, this notion of youthful tectonic activity building the relief of the upland system has been further developed by *Sandiford* [2003], who has suggested as much as half of the present-day relief of the Mount Lofty Ranges is associated with late Neogene reverse faulting, with Quaternary slip at rates locally as high as 50 m Myr^{-1}.

[19] An important aspect of the regional relief relates to basement structure beneath range flanking pediments that bound the Flinders Ranges. These pediments are developed on both exposed basement and thin alluvial fan sequences. Characteristically, the unconformity between the alluvial fan sequences and underlying basement (Figure 5a), dips gently away from the ranges, implying that the long-wavelength surface topography mimics the topography on the basement

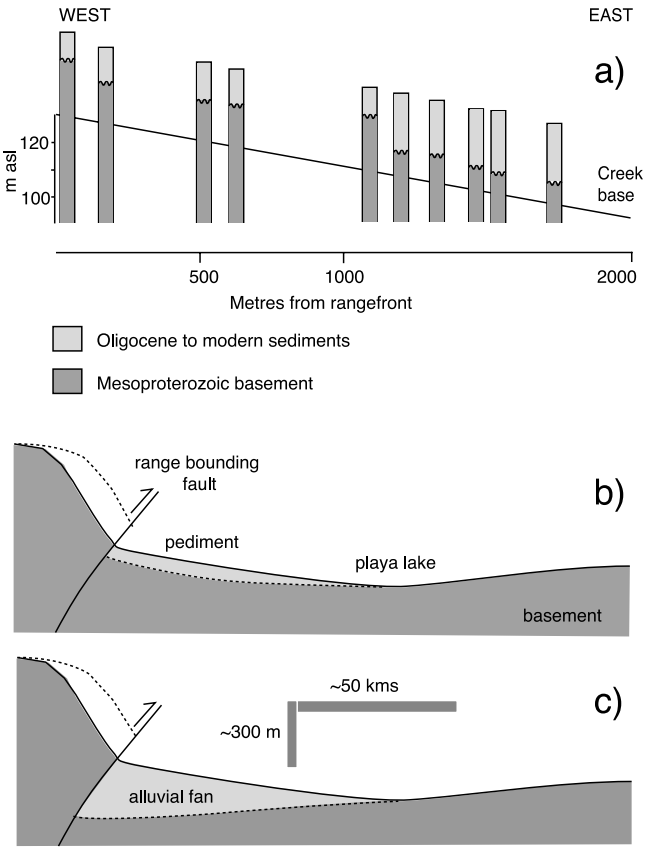

Figure 5. Stratigraphic section from the foreland of the Paralana escarpment and schematic interpretation of the significance of this foreland basin architecture. (a) Manner in which the Mesoproterozoic basement slopes away from the ranges. (b) and (c) Long-wavelength topography and structure of a range flank bounded by reverse faults. The structure of the Flinders Ranges and surrounding playa lake systems resembles Figure 5b in as much as the basement-alluvium interface beneath pediments in the footwall of range bounding faults invariably dips away from the range toward the a topographic minimum located at the site of the playa lake.

surface (Figure 5b), rather than the architecture of flexurally controlled, footwall basins (Figure 5c). This observation has important ramifications for understanding the various modes of active deformation in this region (see section 4).

3.3. Neotectonic Record

[20] Although not widely acknowledged, a number of workers have noted evidence for range-bounding Quaternary faulting within the Flinders and Mount Lofty Ranges [*Sprigg*, 1946; *Williams*, 1973]. Below we briefly describe a few localities that evidence this activity, including previously undocumented localities from the Paralana escarpment in the northern Flinders Ranges and the Burra region in the southern Flinders Ranges (Figure 6, locations as shown on Figure 3).

[21] Along the Paralana escarpment, numerous outcrops attest to active reverse faulting. The most spectacular site, some 4 km northeast of the Paralana Hot Springs near the town of Arkaroola, exposes a thrust slice of Proterozoic quartzite above a footwall comprising titled, angular fan conglomerates of the Pliocene Willawortina Formation underlying a 6 m long wedge of much younger (?late Quaternary) talus that can be traced upward into the active hill scree. The thrust plane dips at 25° to the west, beneath the main topographic edifice of the northern Flinders Ranges. In the alluvial fans outboard of the escarpment the Pliocene Willawortina Formation is up to ~150 m thick [*Callen and Tedford*, 1976], implying in excess of 150 m of post early Pliocene motion on the fault.

[22] In another locality, along the western flank of the ranges in the Wilkatana region, *Williams* [1973] has documented a northwest striking (~330°, dips 46°NE) reverse fault at the apex of the North Wilkatana fan, that places Neoproterozoic Emeroo Quartzite over loosely consolidated talus breccias and river gravels (Figure 6c). The footwall deposits form part of the Late Quaternary Pooraka Formation. An optically stimulated luminescence (OSL) age of 61,000 ± 11,000 years has been obtained from the correlative Pooraka Formation downstream of the fault [*Quigley et al.*, 2005]. Calcareous gouge from the fault plane yielded a radiocarbon date of 23,450 ± 550 years B.P. [*Williams*, 1973], broadly constraining the last faulting event to the ~60–23 ka interval. Steeply southeast plunging lineations on the fault plane indicate reverse-oblique approximately ESE-WNW directed contraction with a measured dip-slip separation of ≥12.0 m and an inferred slip of at least 25.6 m. Geometric analysis of the fault plane in the context of the age data translates to time averaged slip rates of at least 200 m Myr^{-1} and possibly as much as ~400 m Myr^{-1}, although the relative youth of the latest movement suggests that such averaging is inappropriate. A more conservative slip rate of 22–25 m Myr^{-1}, based on the assumption that the footwall fan sequences began accumulating in the early Pliocene is probably more appropriate.

[23] The Burra Fault (Figure 6d) is located several kilometers outboard of the eastern flank of the southern Flinders Ranges. It is exposed at the base of a ~8 m deep erosion canyon incised into range-bounding alluvial fan sequences. The fault comprises a hanging wall of Neoproterozoic Appila Tillite thrust to the northeast over moderately consolidated sediments of the Pooraka Formation. The fault strikes ~140° and dips 38° SW. An OSL date of 85 ± 11 ka has been obtained from the overlying Pooraka Formation, providing a minimum age for the last offset. Regional correlations suggest the footwall Pooraka Formation is likely to be in the age range 90–120 ka, with the slip of ~2.3 m since deposition of that unit translating to a maximum slip rate of ~20 m Myr^{-1}.

[24] We note that the range-bounding faults both within the Flinders Ranges described above, as well as those farther south in the Mount Lofty Ranges (Figure 6c), are clearly reverse while focal mechanisms are dominated by strike-slip mechanisms with just a few reverse mechanisms [e.g., *Clark and Leonard*, 2003]. This is suggestive of a

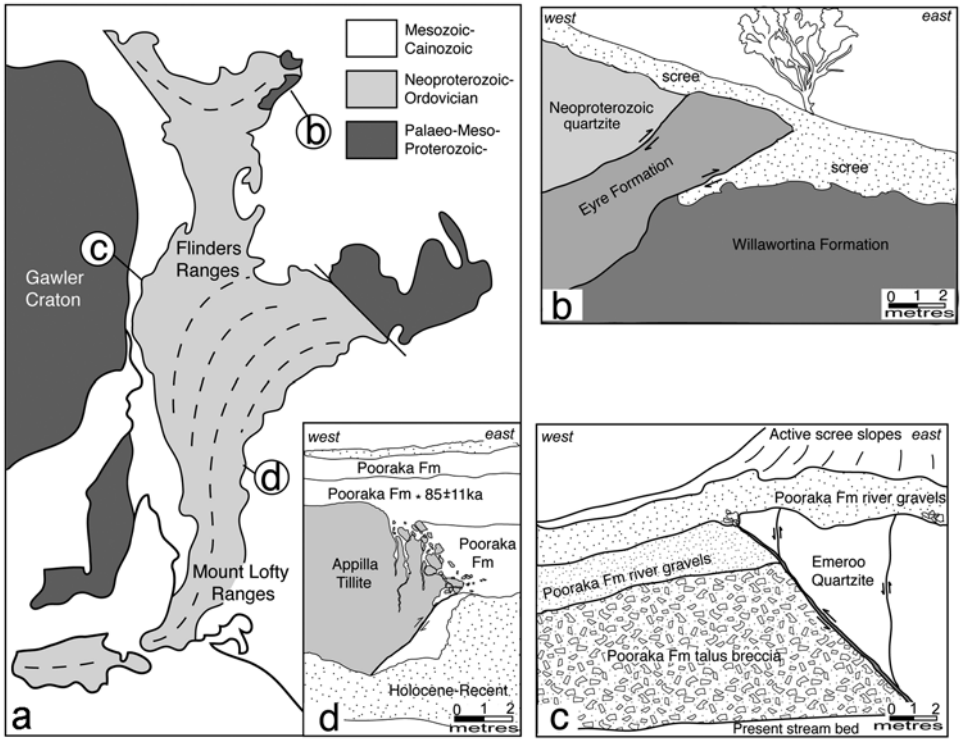

Figure 6. (a) Highly simplified geological map of the Flinders and Mount Lofty ranges region with insets showing sketches of exposures of range bounding thrust faults from (b) Paralana, (c) Wilkatana, and (d) Burra.

topographic partitioning of deformation, with range-bounding faults associated with the largest topographic gradients dominantly reverse, and faults in the interior of the ranges dominantly strike slip. So far, no Quaternary strike-slip faults have been recognized, possibly because without clear vertical offsets of young sediments such faults would not be easily distinguished from older Delamerian structures.

[25] As first noted by *Sandiford* [2003], one of the most important aspects of this recognition of neotectonic fault movement in the Flinders Ranges is that it provides a geological context for understanding the modern seismicity in this region as well as elsewhere in southeast Australia [*Sandiford et al.*, 2004]. At least to first order, the neotectonic slip rates inferred for these faults accord with the estimates of the seismic strain rate detailed in section 2.1 suggesting that despite the inherent uncertainties, useful estimates of seismic strain obtained by summation of seismic moment release may be made in more active parts of SCRs.

3.4. South Australian Gravity Field

[26] As with the gravity fields from many continental regions, the South Australian gravity field displays a complex pattern with somewhat noisy signals. As noted by *Wellman and Greenhalgh* [1988], the Flinders and Mount Lofty Ranges and surrounding basins are characterized by a series of subparallel Bouguer anomalies roughly aligned with the topography (Figure 7). The axis of the central and northern Flinders Ranges is coincident with a generally positive, though disrupted, Bouguer gravity anomaly of amplitude ~20 mGal. Within the ranges a set of distinctive linear gravity lows correlate with narrow, anomalously thick Neoproterozoic successions, related to the original rift geometry. For example, the NW trending gravity low of amplitude 20 mGal in the northwestern part of the ranges (north of 31°S) relates to a graben of Burra group sediments bounded by the Norwest fault [*Paul et al.*, 1999]. Similarly, the gravity low along the western range front between the central and southern Flinders Ranges (between 32° and 34°S) can be related to a narrow depocenter developed during the Sturtian glacial interval [*Preiss*, 1987].

[27] As shown most clearly in Figure 4b, a broad gravity low (amplitude ~20 mGal) occurs to the east of the northern Flinders Ranges in the vicinity of Lake Frome. Equally, on the western side of the ranges an elongate gravity low (~15 mGal) extends from Lake Torrens south to the western range flank of the ranges in the vicinity of Wilkatana, thus defining a sinusoidal gravity pattern across the axis of the ranges and flanking playa lake systems.

[28] The first-order positive correlation between topography and Bouguer gravity anomalies over the axis of the ranges and flanking basins (Figure 4), particularly in the northern Flinders Ranges, is intriguing, since this not what is expected for crustal deformation, where isostatic compensation is common. While this may simply may reflect the fact that the isostatic Bouguer anomaly is lost in inherited noise, it does raise the possibility that the Flinders Ranges forms part of a much longer wavelength

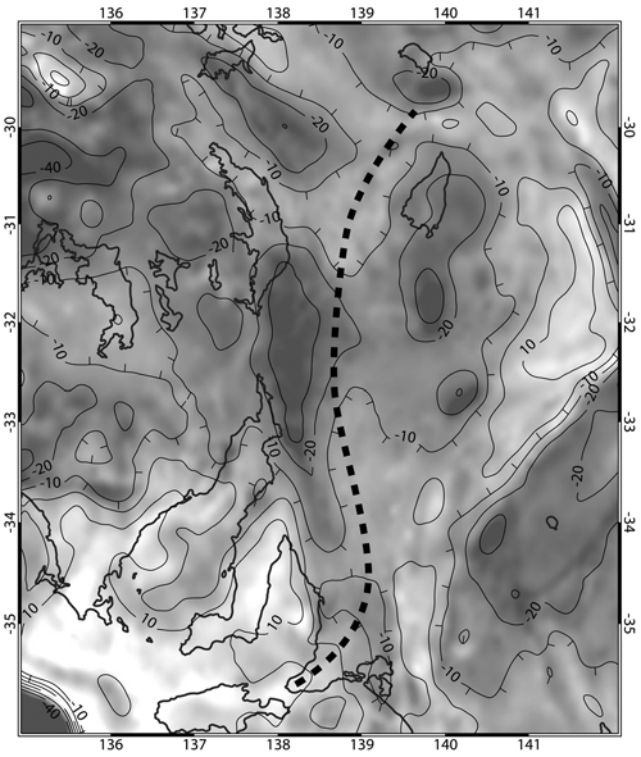

Figure 7. South Australian Bouguer gravity field. Dashed line shows the topographic axis of the ranges, and for the Flinders Ranges (north of about 33°30′S), coincides with a weak positive Bouguer gravity anomaly. Brighter colors represent positive Bouguer gravity signal, while darker colors represent regions of negative Bouguer gravity anomaly.

topographic response to the contemporary stress field, something to which we return in section 4.2.

4. Modes of Deformation

4.1. Controls on Localized Lithospheric Failure

[29] The pattern of seismicity shown in Figure 3, together with the existence of range-bounding Quaternary thrust faults, clearly highlights the relatively intense nature of active deformation in the Flinders Ranges, raising the question of what factors contribute to the focusing of this activity? As outlined earlier, previous work has shown that the elevated heat flow in the vicinity of the Flinders Ranges can be attributed to exceptional heat production in Mesoproterozoic basement that must be more deeply buried in the crust beneath the Flinders Ranges by virtue of the Neoproterozoic sedimentary cover. This sedimentary cover typically exceeds 5 km in thickness, and hence we pose the question here whether the first-order thermal response of the lithosphere to the burial of hot basement beneath a sedimentary cover is sufficient to locally weaken the lithosphere?

[30] A fundamental but not widely appreciated aspect of continental conductive thermal regimes is the fact that both the amount of heat sources in the mid to upper crust and the way they are distributed with depth impacts on the thermal structure of the deeper crust and upper mantle. As shown by *Sandiford and McLaren* [2002] a very simple parameterization illustrates this effect: the temperature at any depth z contributed by heat production above is

$$T_z = \frac{q_c\, h}{k} \tag{4}$$

where h is a measure of the effective depth of the overlying heat production, q_c is the vertically integrated abundance of that heat production and k is the characteristic thermal conductivity. Thus the change in the conductive temperature at any depth z due to changes in the distribution of overlying heat production parameters, h and q_c is just

$$\Delta T_z = \frac{q_c'\, \Delta h}{k} + \frac{\Delta q_c\, h'}{k} \tag{5}$$

where q_c' and h' are reference values.

[31] Thus there are two potential sources of elevated temperatures in the deep crust and upper mantle beneath the Flinders Ranges: (1) the additional heat sources in the crust responsible for the heat flow anomaly ($\Delta q_c \sim 15$–30 mW m^{-2}) and (2) the relatively deeper burial of these heat source beneath the Flinders Ranges by virtue of the Neoproterozoic cover sequence ($\Delta h \sim 5$ km). For the Flinders Ranges the reference value, q'_c, is given by the crustal contributions to heat flow in the adjacent regions and is estimated to be ~40 mW m^{-2}. The reference value, h', is not directly constrained by available measurements but we use a value of 5 km which implies a very shallow concentration of heat production, consistent with the relatively high values of surface heat production observed throughout the region [*Neumann et al.*, 2000]. Assuming a thermal conductivity of 3 W m^{-1} K^{-1}, these values yield ΔT_z = ~90–120°C implying a significantly hotter upper mantle beneath the Flinders Ranges than the adjacent areas where heat flow is lower and heat sources must be shallower.

[32] Lithospheric rheology is generally believed to be temperature-dependent and particularly sensitive to the thermal state of the upper mantle [*Sonder and England*, 1986], and such inferred temperature variations should impact on the mechanical state of the lithosphere. To investigate this we use a popular, generalized model for lithospheric rheology, the so-called ''Brace-Goetze'' model [*Brace and Kohlstedt*, 1980; *Molnar*, 1989]. In this model the lithosphere is assumed to deform by a combination of pressure (or depth) dependent frictional sliding and temperature and stress-dependent power law and Dorn law creep mechanisms. *Sandiford et al.* [1998] have previously investigated the rheological response of the Brace-Goetze lithosphere to the burial of a radiogenic basement beneath a cover sequence, while *Sandiford and McLaren* [2002] have provided a more general analysis of the rheological consequences of changes in heat source parameters, h and q_c, and we reproduce their results here in Figure 8. The interested reader is referred to both *Sandiford et al.* [1998] and *Sandiford and McLaren* [2002] for full details of the

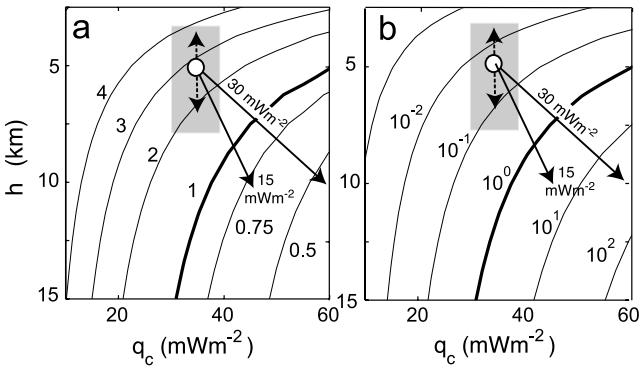

Figure 8. (a) The h-q_c plane contoured for integrated lithospheric compressional strength. (b) The h-q_c plane contoured for rate of deformation subject to an imposed compressional tectonic load adapted from *Sandiford and McLaren* [2002]. The assumed rheology is that of the Brace-Goetze lithosphere in which deformation is governed by a combination of frictional sliding and temperature-dependent creep. The strength parameters are shown normalized against a configuration characterized by q_c = 45 mW m^{-2} and h = 7 km (bold lines). The arrowed lines show that a heat flow anomaly of between 15 and 30 mW m^{-2} resulting from heat source buried more deeply in the crust by 5 km (as appropriate for the Flinders Ranges) leads to a reduction in bulk strength by a factor of ~5 (Figure 8a) and an increase in strain rates subject to an imposed load of more than 2 orders of magnitude (Figure 8b). Note that the effective depth of the heat production, h, outside the heat flow anomaly is not well constrained (as indicated by the shaded region), but this uncertainty does not translate to significant variations in the calculated strength differences associated with the Flinders Ranges heat flow anomaly. Further, while the absolute values of strength are sensitive to a large number of assumed parameters including thermal conductivity (here k = 3 W m^{-1} K^{-1}) and mantle heat flux (here q_m = 30 mW m^{-2}), as well as the material parameters constraining creep and frictional sliding of crustal and mantle rocks, the relative strength variations due to changes in h-q_c parameters are relatively robust.

model parameters. Figure 8 shows that a heat flow anomaly of about 15–30 mW m^{-2} resulting from heat source buried more deeply in the crust by 5 km (as appropriate for the Flinders Ranges leads to a reduction in bulk strength of a Brace-Goetze lithosphere by a factor of between 2 and 5 (Figure 8a) and an increase in strain rates subject to an imposed load of 2 orders of magnitude or more (Figure 8b).

[33] Strictly, equations (4) and (5) only hold in the one-dimensional (1-D) limit where there is no lateral heat flow and the Flinders Ranges are sufficiently narrow that the effective heating of the deep crust and upper mantle beneath the Flinders Ranges will be ameliorated by lateral heat flow. To explore this we use a 2-D numerical model based on *Hansen and Nielsen*'s [2003] formulation (to which the reader is referred to for a full description) of a finite element algorithm solving for elastoplastoviscous deformation and transient heat flow for a Brace-Goetze rheology (see Table 1 for summary of rheological properties). Plastic deformation occurs when the pressure-dependent yield strength of the rock is exceeded and simulates fracturing. Viscous deformation follows a temperature, strain rate and rock type dependent Dorn creep power law rheology [*Ranalli*, 1995]. Buoyancy forces act at density contrast interfaces located at the surface, basement, midcrust, Moho and the base of the lithosphere. Erosion is modeled using a diffusion equation with a source term enabling the transport of sediments to and from the model profile. We model a 500 km wide and 100 km deep domain discretized into a finite element mesh with 2592 triangular elements. The modeled lithosphere profile is initially partitioned into four rheological layers consisting of sediments, upper crust (20 km wet quartz), lower crust (15 km wet feldspar) and lithospheric mantle (65 km dry olivine). The rheological properties of these materials are listed in Table 1 and are dependent on temperature, pressure, composition, and deviatoric stress magnitudes and not given as prior constraints in any element [*Hansen and Nielsen*, 2003]. Vertical boundaries of the model are axes of symmetry. Deformation is induced by lateral displacement, with no tilt, of the right boundary (Figure 9). Upper and lower thermal boundary conditions are constant surface temperature and constant basal heat flux, respectively.

[34] Our model formulation is motivated by the recognition that the tectonic history of the Flinders Ranges reflects a multistage inversion of a Neoproterozoic rift basin formed on older crust highly enriched in heat producing elements [e.g., *Sandiford et al.*, 1998; *Neumann et al.*, 2000]. In particular, the following phases are relevant to the first-order tectonic history of the Flinders Ranges: (1) Neoproterozoic basin formation (~800–550 Ma) with crustal thinning and sediment deposition, (2) Delamerian inversion (~500–450 Ma), followed by (3) erosion and sediment redistribution to remove Delamerian topography (~450–300 Ma) prior to the Mesozoic and (4) a neotectonic "inversion" associated with the formation/amplification of the present-day topography (~10–0 Ma. In order to reproduce the heat flow anomaly associated with the Flinders Ranges, a zone of high basement heat production is included, as shown in Figure 9:

$$H(x,z) = H_0 \exp\left(\frac{-(x-x_0)^2}{h_x^2}\right) \exp\left(\frac{-(z-z_0)^2}{h_z^2}\right) \qquad (6)$$

where z_0 is the depth of the locus of enriched heat production; H_0 is the heat production maximum at the locus of the anomaly, i.e., at $z = z_0$ and $x = x_0$, at the center of the model; and h_z and h_x provide a measure of spread of the heat distribution in the vertical and horizontal directions. The anomaly is superposed on a background heat production field with model parameters chosen to produce a vertically integrated crustal heat flow contribution beneath the basin centre of 120 mW m^{-2}, superimposed on a background heat flow contribution of 60 mW m^{-2}.

[35] We impose boundary conditions that encapsulate the multiphase inversion history of the Flinders Ranges, condensed into a model run time of a few hundred million

Table 1. Finite Element Model Parameters[a]

Parameter	Symbol	Wet Quartz	Wet Feldspar	Dry Olivine	Reference
Young's modulus	E, Pa	10^{11}	10^{11}	10^{11}	1
Poisson's ratio	ν	0.25	0.25	0.25	1
Creep parameter	B, MPa $s^{1/n}$	29.6	14.0	0.0258	2, 3
Creep parameter	Q, kJ mol^{-1}	160	235	535	2, 3
Creep parameter	n	2.4	3.9	3.5	2, 3
Angle of internal friction	ϕ	30	30	30	1
Cohesion	C, MPa	5.0	5.0	5.0	1
High-pressure fracturing	p^H, MPa	800	800	800	1
Duvaut-Lions relaxation time	ζ, years	1000	1000	1000	1
Density at 0°C	ρ_0, kg m^{-3}	2800	2900	3400	1
Thermal conductivity	k, W m^{-1} K	3.0	2.3	4.0	4
Specific heat	c, J kg^{-1} K^{-1}	850	900	1000	4
Heat production rate	A, μW m^{-3}	1.3	0.3	0.01	4
Thermal expansion coefficient	α, K^{-1}	3.2×10^{-5}	3.2×10^{-5}	3.2×10^{-5}	1

[a]After *Hansen and Nielsen* [2003]. The references are 1, *Jaeger and Cook* [1969]; 2, *Ranalli* [1995], 3, *Bassi* [1991]; 4, *Nielsen and Hansen* [2000]. In the sediments, $\rho_0 = 2300$ kg m^{-3}, $k = 2.0$ W m^{-1} K^{-1}, $A = 1.0$ μW m^{-3}, and $c = 900$ J kg^{-1} K^{-1}. The porosity of sediment decreases with burial according to $\Phi = \Phi_0 \exp(z/2\text{ km})$, where Φ_0 is surface porosity and z is maximal burial depth.

years, rather than the full ~800 Myr history since initial Neoproterozoic rifting. This temporal "short cut" is justified so long as we allow time intervals sufficient for lithospheric-scale thermal equilibration following tectonic activity, for example, *Braun and Beaumont* [1987], who show that the time required for a thermally and mechanically disturbed piece of continental lithosphere to fully reequilibrate following perturbation is in the order of 60 Myr. We have used time intervals of 60 Myr to separate the thermally discrete tectonic episodes in our model.

[36] The initial model phase simulates formation of the rift succession by extensional displacement of the model's lateral boundaries at a rate of 3 km Myr^{-1} for 25 Myr (Figure 10). Velocities are then reduced linearly over 5 Myr until the boundaries become fixed at 30 Myr. Postrift, sag phase, sedimentation continues for a further 60 Myr, when the basin is approximately 9 km deep and 200 km wide (Figure 11b), appropriate to some of the deeper parts of the Neoproterozoic rift succession [*Preiss*, 1987; *Paul et al.*, 1999]. The 60 Myr period following the cessation of rifting allows thermal reequilibration, and dissipation of all residual strains resulting from extensional stresses. A first phase of inversion, simulating "Delamerian" inversion, is initiated at 90 Myr by imposing a 15% shortening of the sedimentary package, consistent with the estimates for bulk Delamerian shortening of *Paul et al.* [1999]. The shortening is imposed over a period of 20 Myr as shown in Figure 10 and is followed by a further 60 Myr period of thermal reequilibration. While there are no definitive estimates of the total shortening associated with the neotectonic activity in the northern Flinders Ranges, an estimate can be derived by extrapolating seismogenic strain rates (~0.5 km Myr^{-1})

Table 2. Flexural Model Parameters

Parameter	Value
Densities, kg m^{-3}	
Sediment	2700
Crust	2900
Mantle	3200
Flexural rigidity, N m	10^{22}
Kinematic stretching factor	2.0
Initial crustal thickness, km	40

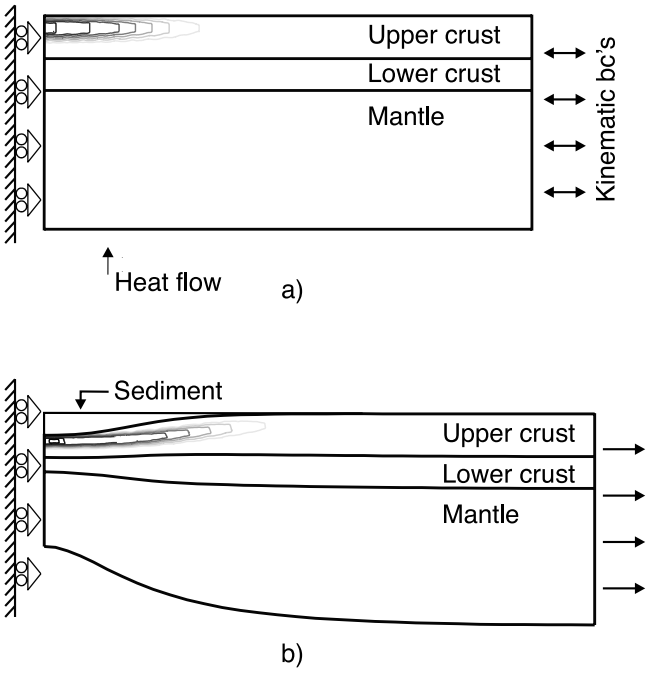

Figure 9. Schematic illustration of the initial geometry of the finite element model used to investigate possible first-order dynamics controlling the neotectonic deformation localized in the Flinders Ranges. The model is laterally homogeneous except in the central portion of the upper crust where a zone of intensified heat production is included. At its centre, the heat production anomaly contributes (along with the basal heat flow) to a surface heat flow of ~120 mW m^{-2}. The background heat production contributes (along with the basal heat flow) to a surface heat flow of 60 mW m^{-2}.

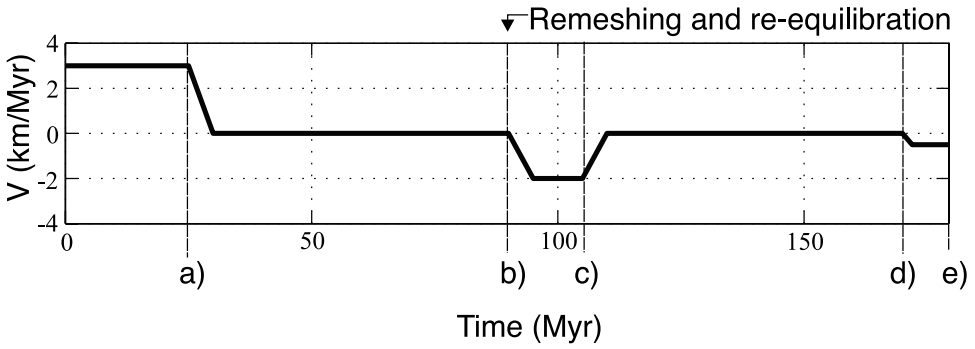

Figure 10. Illustration of the kinematic boundary conditions enforced on the thermomechanical model through time. The *x* axis shows the models progression through time, while the *y* axis shows the magnitude, and nature, of displacement of the model boundaries. Positive *y* axis values indicate extension, while negative values represent compression. Letters refer to the corresponding panel in Figure 11.

over the likely period of deformation, assumed to be of the order of 5–10 Myr [*Sandiford*, 2003]. We impose this in the model by linearly increasing the boundary velocity to 0.5 km Myr^{-1} over 2 Myr and maintaining this velocity for a further 8 Myr (Figure 10). Following initial stretching and thermal subsidence the model is remeshed as appropriate to the fully restored mantle lithosphere (see Figures 11b and 11c).

[37] Figure 11 shows results for critical steps in the evolution of the model. The thermal weakening effect of the high crustal heat production is clearly effective in localizing the initial phase of stretching (Figure 11a) as well as during subsequent compressive strains (Figures 11c and 11e). During subsequent Delamerian shortening, crustal strains tend to be localized beneath the basin flanks (Figure 11c), in accord with the generalized basin inversion model predictions of *Hansen and Nielsen* [2002, 2003] and *Sandiford* [1999]. Following the localization of strains and building of topography during the inversion event, Delamerian topography is eroded and redistributed in the flanking basins. All topography is effectively eroded away, resulting in a flat model surface, after a few tens of millions years of model time. The pulse of neotectonic compression, imposed on the lithospheric structure shown in Figure 11d, again localizes strains within the thermally weakened region underlying the Neoproterozoic basin, particularly beneath the rift flanks. Again topography is built as the package is uplifted while the flanking areas are flexurally downwarped. The marginal troughs progressively deepen and there lateral extent increases with continued neotectonic compression, ultimately producing a regional topographic pattern that closely resembles the long-wavelength pattern observed in the topographically depressed regions now occupied by playa lake systems.

[38] The model results shown in Figure 11 highlight the effectiveness of a basement heat flow anomaly in localizing deformation, through a multistage inversion history spanning many hundreds of millions of years. An implication of this modeling is that the localized active deformation of the Flinders Ranges can be accounted for by the thermal consequences of crustal heat production. In order to be sure of the role the heat flow anomaly plays in the tectonic history of the region we have run an identical model with the heat flow anomaly removed. The results of this model substantiate the observation that tectonic localization results from the inclusion of a heat anomaly. With the anomaly removed, deformation is accommodated by bulk pure shear without any localization (since nonlinear effects such as strain softening are not included, only the thermal anomaly introduces localizing effects in the initial phases of the model). Consequently, the surface uniformly subsides during extension and later rises during compression, with no relief development in the modeled domain.

4.2. Role of Lithospheric Flexure

[39] While the model results shown in Figure 11, appealingly account for the localized nature of historical seismicity and, in a broader sense, the distribution of Quaternary faulting in the Flinders Ranges, they do not address the observed gravity pattern. In particular, the weak positive gravity anomaly over the Flinders Ranges and its coincidence with topography at long wavelengths. This geophysical signal suggests that as well as the seismogenic mode of active deformation, there may be a component of lithospheric flexure in the region. Here we explore the likely geophysical response to a purely elastic mode of deformation appropriate to the multiphase inversion history of the Flinders Ranges outlined above.

[40] Lithospheric-scale flexure is a controversial deformation mode that has been invoked by a variety of workers to explain periodic undulatory patterns of gravity and topography in a variety of settings [*Cloetingh et al.*, 1999]. For example, the occurrence of intraplate flexure of the oceanic lithosphere is firmly established in the

Figure 11. Five-step cartoon showing the most important steps in thermomechanical model evolution. Each figure shows strain rate contours and topography. Refer to timeline in Figure 10 for relative timing of each step. (a) Late stage of rifting. (b) Basin immediately prior to Delamerian compression and before remeshing. (c) Late stage of Delamerian compression. (d) Basin just before neotectonic compression. (e) Late stage of neotectonic compression.

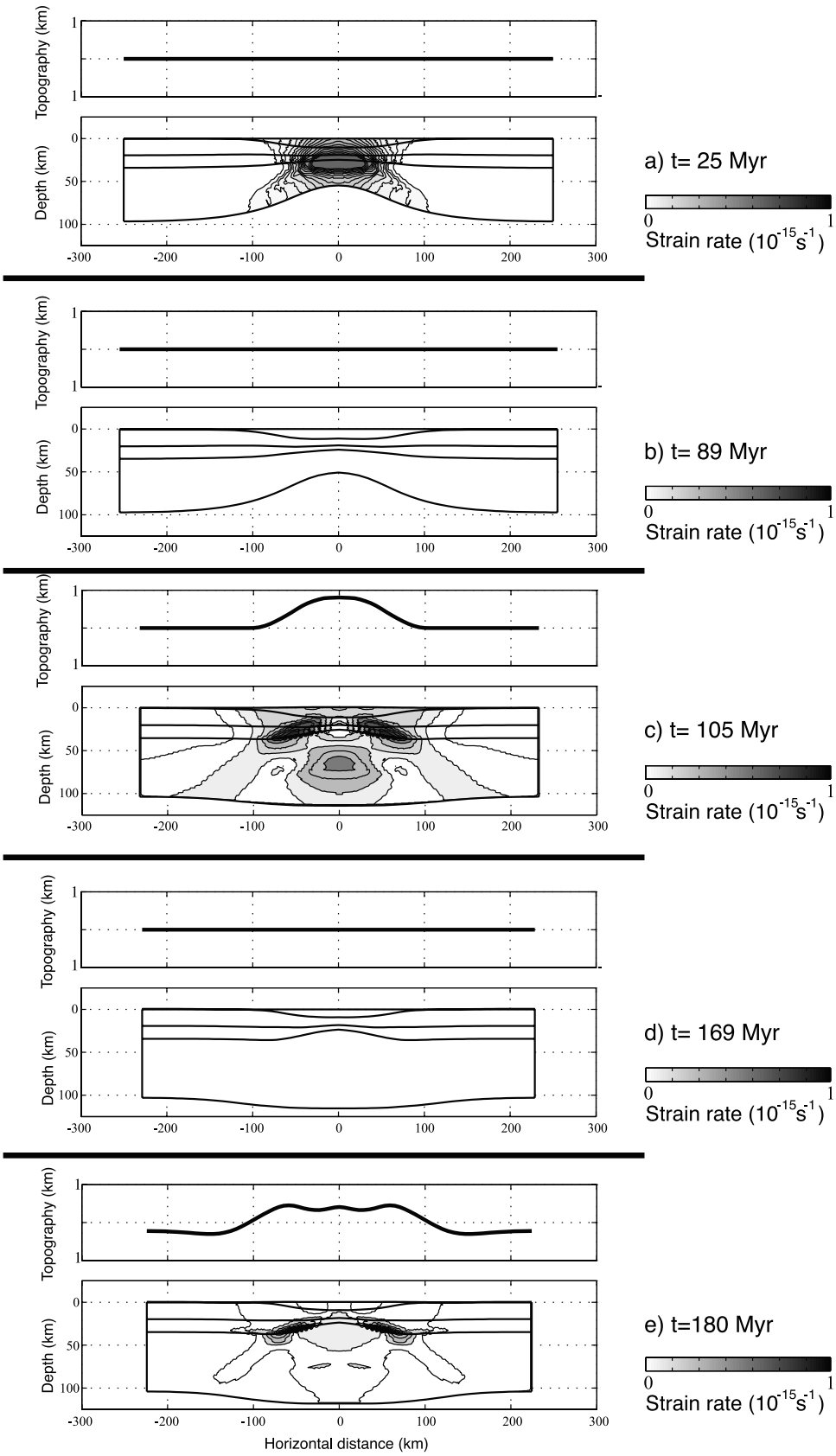
Topography (km)
Depth (km)
a) t= 25 Myr
b) t= 89 Myr
c) t= 105 Myr
d) t= 169 Myr
e) t=180 Myr
Strain rate ($10^{-15}s^{-1}$)
Horizontal distance (km)

Figure 11

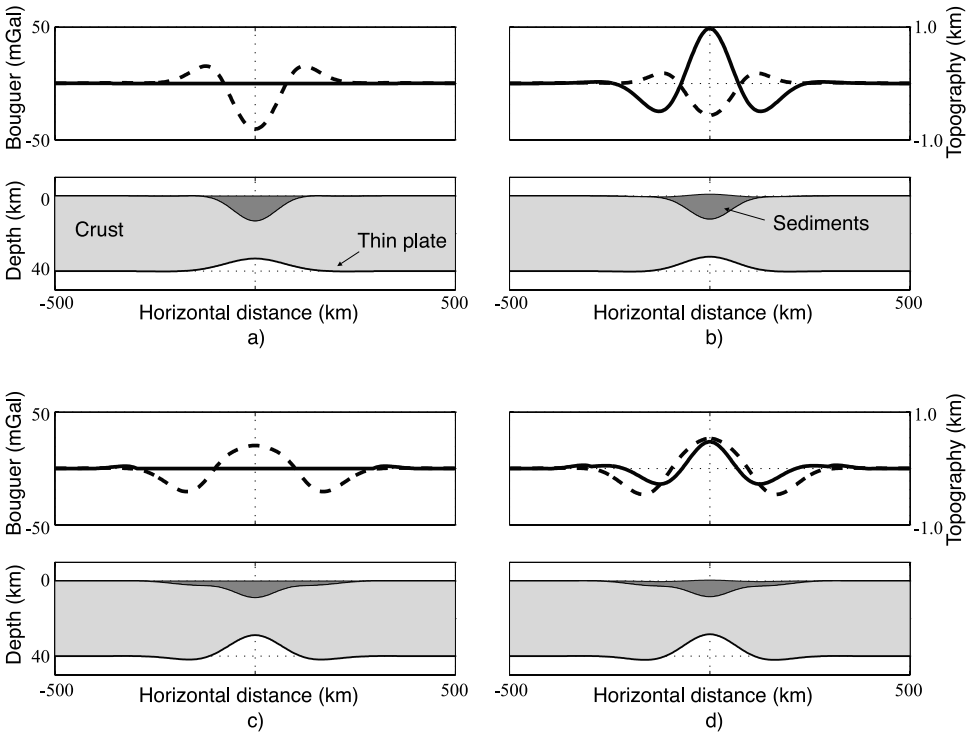

Figure 12. Elastic thin plate model with coinciding gravity and topography highs. The thin plate model evolves in 4 phases. Solid line is topography and the dashed line is the gravity signal. (a) Initial basin formed by thinning the crust kinematically and the elastic plate, positioned at Moho level, is deflected upward due to sediment-crust density differences, (b) a topographic high (inversion zone) flanked by marginal depressions results from horizontal compression, (c) redistribution of sediments by erosion and deposition flips the predicted Bouguer anomaly forming a gravity high in the inverted basin, and (d) a second horizontal stress build-up creates topography without significantly affecting the gravity signal.

northeastern Indian Ocean [*Geller et al.*, 1983]. In this example, bathymetric anomalies reveal subparallel undulations of the oceanic bed with wavelengths of 100 to 300 km, and amplitudes of up to 1 km. *Stephenson and Cloetingh* [1991] have argued for lithospheric flexure to explain the unusual gravity pattern in central Australia where gravity highs with amplitude +150 mGal coincide with regions of structural inversion. Highlighting the earlier work of *Lambeck* [1983], *Stephenson and Cloetingh* [1991] argued that the N-S trending late Proterozoic to Carboniferous sedimentary basins and intervening basement complexes of central Australia reflect lithospheric flexure in the presence of significant and long-lived horizontal compressional stresses.

[41] To test the role of lithospheric flexure as a mode of deformation responsible for the geophysical signals in the Flinders Ranges, we follow the methodology and model assumptions of *Stephenson and Cloetingh* [1991], treating the lithosphere as a thin elastic plate with characteristic stiffness, loaded by horizontal tectonic forces and vertical buoyancy forces. Because of prior history related to older tectonic activity, the plate is predeflected. We assume the predeflection can be ascribed to an elastic beam in the uppermost mantle, based on most current views about the vertical strength distribution in the lithosphere [e.g., *Brace and Kohlstedt*, 1980] (see further discussions by *Karner* [1986] and *Karner et al.* [1993]). First-order constraints on the elastic thickness of the Australian lithosphere are provided by long-wavelength coherence studies [*Zuber et al.*, 1989; *Simons et al.*, 2000], with *Simons et al.* [2000] suggesting that South Australia is characterized by an elastic thickness in the order of 40 km. Given the anomalous heat flow in the vicinity of the Flinders Ranges we anticipate that the elastic thickness is lower than average, and in the calculations below we assume an elastic thickness of 30 km. We simulate the multiphase inversion history of the Flinders Ranges by varying the horizontal and vertical forces applied to the thin elastic plate. The Bouguer gravity response is calculated through the integration of density differences between sediments and crust, as well as crust and mantle along seventy horizontal points at the top of the model. Densities as well as the flexural parameters used in these calculations are listed in Table 2.

[42] The general character of the elastic response to each of the steps in the deformation history of the region is summarized in Figure 12 and briefly outlined below. In the initial phase, basin formation leads to an upward "predeflection" reflecting the shallowing of the upper mantle beneath the thinned crust, and a Bouguer gravity response characterized by a short-wavelength negative anomaly

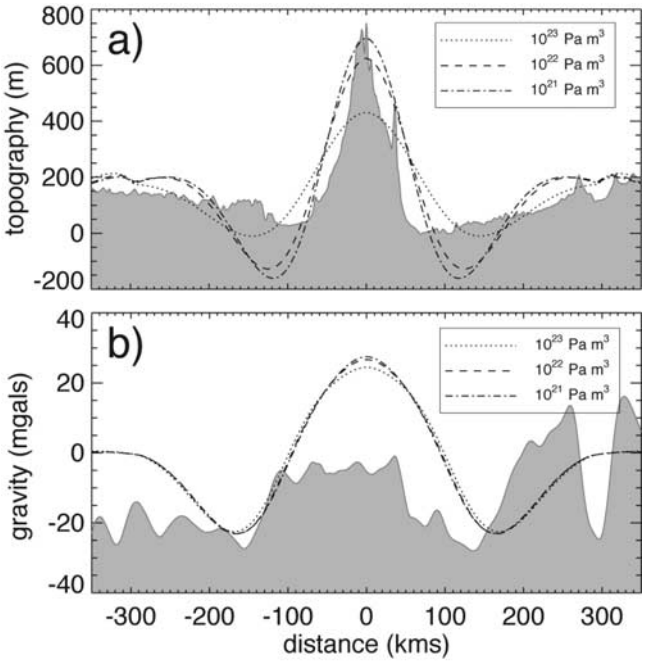

Figure 13. Comparison of observed (a) topography and (b) Bouguer gravity field with predictions of thin elastic plate failure models, using different values of flexural rigidity.

(reflecting the low-density basin fill) superimposed on a longer wavelength positive signal arising from the dense upper mantle beneath the basin (Figure 12a). Delamerian inversion (achieved by imposing an in-plane load of 1×10^{13} N m^{-1}) further amplifies this preexisting deflection in proportion to the plate's curvature. Thus the Moho is further elevated and surface topography created beneath the Neoproterozoic basin centre, while the basin flanks are deflected downward leading to formation of flanking basins (Figure 12b). Significant vertical displacements and changes to the gravity signal accompany erosion of Delamerian topography as the sediments are redistributed to fill the flanking basins (Figure 12c). The changes in the vertical restoring forces result in further downward deflection of the rift flanks and uplift in the basin centre. By the time surface processes have effectively smoothed all Delamerian topography, the gravity signal is reversed, showing a positive anomaly centered above the remnant Neoproterozoic basin between two negative anomalies parallel to the rift flanks (Figure 12c). The final, neotectonic, compressive episode (achieved by imposing an in-plane load of 5×10^{12} N m^{-1}), induces uplift of the remnant axial basin and depression of flanking "basins" without significantly disturbing the gravity signal resulting in coincident positive gravity and topography anomalies (Figure 12d). The magnitude of both the amplitude and wavelength of the flexural response is clearly dependent on the assumed flexural parameters (e.g., Figure 13a), as well as the imposed load, and prior loading history. Thus it is important to recognize that we have no independent constraints on the magnitude of present-day in plane stress to corroborate the veracity of the imposed load (see section 5). We do, however, have first-order estimates of effective elastic thickness [e.g., *Simons et al.*, 2000] and using published values in our modeling yields results largely consistent with the observed topographic and gravity fields. The amplitude of the associated Bouguer gravity anomaly is rather less sensitive than topography to variations in flexural parameters (e.g., Figure 13b), with the predicted amplitude of 50 mGal associated with relief of 500–1000 m.

[43] Importantly, despite the inherent simplicity of the flexural model outlined above, the final configuration of gravity and topography (Figure 12d) shows some remarkable parallels with the observations. Most importantly, the foreland is characterized by a preneotectonic surface that slopes gently away from the main topographic edifice toward depocenters located ~100 km outboard of the main range. While the predicted axial relief (~800 m), reflecting the imposed load, corresponds closely to the observed relief, the ~300 m relief between the flexural depressions and outer bulges (Figure 12d), is ~2 times that observed. In part, this may be attributed to the partial infilling with Neogene successions in the Torrens and Frome basins locally in excess of 100 m thick [*Alley and Lindsay*, 1995]. Alternatively, it may imply that the applied modeled load (5×10^{12} N m^{-1}) is too high.

5. Discussion

[44] Both geological and geophysical observations in the Flinders Ranges suggest significant ongoing intraplate deformation within the Australian continent of much greater complexity and intensity than is usually accorded to views on contemporary Australian geology. Of particular relevance to understanding this deformation are the distribution of seismicity, the Quaternary faulting record, the pattern of Bouguer gravity, and the architecture of the surrounding flexural basins. These features provide important insights into the modes of active deformation responsible for ongoing seismicity and relief generation in this region. The weak positive Bouguer gravity signal and the unusual flexural basin architecture imply a significant role of low-amplitude lithospheric flexure, while the distribution of seismicity and record of ongoing faulting imply seismogenic strain accumulation at low, yet significant rates (~10^{-16} s^{-1}). While lithospheric flexure is usually related to an elastic mode of deformation, it is more appropriately ascribed to deformation of lithosphere characterized by a plastic yield stress and significant strength contrasts [e.g., *Gerbault*, 2000]. In the following discussion we review some of the important insights provided by our numerical modeling of these deformation modes, which we refer to as the "flexure mode" and the "seismogenic mode," respectively, while recognizing that in nature they form part of a continuous response spectrum [e.g., *Gerbault*, 2000].

[45] An important result of our modeling relates to the spatial pattern of topography. In each mode, the generation of relief is intimately linked to the prior tectonic history and the inherited geochemical make up of the crust. We have shown how the amplification of instabilities in the flexure mode can be related to the distribution of embedded

membrane stresses which provide a predeflection consequent upon prior history. The existence of predeflection related to earlier basin formation restricts the positive topographic relief to the axis of the former basin, while a two-stage inversion history, and subsequent removal of topography is a crucial factor leading to the positive Bouguer gravity anomaly coincident with positive relief. In the seismogenic mode, localization of lithospheric failure can be attributed to lateral variations in lithospheric strength imposed by variations in the thermal property structure of the crust related to (1) unusually elevated abundances of heat producing elements and (2) the redistribution of the heat producing elements during prior tectonic structuring, particularly during basin formation.

[46] While the accumulation of significant seismogenic strain in the presence of long-wavelength lithospheric-scale flexing has been documented from an oceanic setting in the central Indian Ocean [*Weissel et al.*, 1980], it remains controversial in the continents [see *Cloetingh et al.*, 1999]. Such flexure requires a stratified system with significant strength contrasts (i.e., effective viscosity ratios of 10^3 [*Gerbault et al.*, 2003]). In the flexure mode, instabilities typically amplify at wavelengths ~5 times the thickness of the "stiff" layer [*Gerbault et al.*, 2003]. For the Flinders Ranges, the wavelength of flexure implied by the distribution of the playa lakes is ~150 km, implying a layer thickness of around 30 km, close to the crustal thickness in this region. Assuming that dissipation occurs by a viscous response beneath the stiff layer, then it seems probable that the thermal structure of the upper mantle beneath the Flinders Ranges may have played a crucial role in facilitating this mode of deformation, by limiting the strength of the upper mantle.

[47] Together with previous plate-scale modeling studies [*Reynolds et al.*, 2002; *Sandiford et al.*, 2004, 2005], our analysis provides further constraints on the question of the stress magnitudes responsible for active deformation in the Flinders Ranges. Numerical modeling of the intraplate stress field by *Reynolds et al.* [2002] and *Sandiford et al.* [2004] predicted $S_{H\max}$ magnitudes ~25 MPa (averaged over a 100 km thick lithosphere) in the vicinity of the Flinders Ranges. If supported by a ~30 km thick stiff layer, the effective stress magnitudes would be ~75 MPa. Such stress magnitudes are significantly lower than most workers suggest are needed for the amplification of lithospheric flexural instabilities [e.g., *Gerbault*, 2000], although within the range suggested by *Martinod and Molnar* [1995]. Moreover, in the central Indian Ocean (where consensus is that flexure is occurring) the *Sandiford et al.* [2005] $S_{H\max}$ magnitudes are only ~40 MPa averaged over a 100 km thick lithosphere. Here the characteristic flexural wavelength of about 200 km implies layer thickness of 40 km with effective stress magnitudes 100 MPa, only slightly greater than we predict for the Flinders Ranges. These observations also highlight the fact that both regions (the Flinders Ranges and central Indian Ocean) form part of the same fast moving tectonic plate, which is in a state of significant compression by virtue of the way driving torques are balanced by plate boundary collisions [e.g., *Coblentz et al.*, 1995]. Noting the different inferred wavelengths of the flexural instabilities in these two regions, the stress magnitudes within the stiffest layers are probably not significantly different.

[48] On the basis of regional geological constraints pertaining to timing of neotectonic activity across southeastern Australia, *Sandiford et al.* [2004] have argued that the current tectonic regime is essentially a late Neogene phenomenon, reflecting changes in the Pacific-Australian plate coupling at around 10–6 Ma. An older inception of the basins surrounding the Flinders Ranges is suggested by early to mid-Neogene sediments with thicknesses of up to ~100 m in these basins [e.g., *Alley and Lindsay*, 1995]. We would expect that the flexure mode might generate relief in the vicinity of the Flinders Ranges, in response to any significant regional compression in the plate. In this respect, the stress regime within Australia is believed to have been dominated by compression from the mid-Eocene when fast spreading commenced in the Indian Ocean, and Australia commenced its rapid (6–7 cm yr^{-1}) northward drift [e.g., *Sandiford et al.*, 1995]. Thus it seems quite conceivable that the flexure mode is associated with a staged relief generation through much of the Cenozoic. During the Neogene, and particularly over the last 10 Myr, stress levels in the Indo-Australian plate have increased due to increased plate boundary forcing. Our paradigm of the lithosphere in the vicinity of the Flinders Ranges initially responding to the new stress regime by broad flexure, fits with the work of *Cloetingh et al.* [1999], who argue that lithospheric "flexure" is a standard response to recently induced compressional stress fields. They also suggest that following an initial flexural response, deformation becomes localized leading to localized failure and, once strains are large enough, orogeny. Such a sequence of deformation resembles very closely the recent tectonic history of the Flinders Ranges, although at strain rates of $\sim 10^{-16}$ s^{-1} orogeny is still many millions of years into the future!

[49] In summary, we propose that the following sequence of deformation has contributed to building the present-day relief of the Flinders Ranges. Following the establishment of the current compressive Indo-Australian stress field at ~10–6 Ma, the lithosphere of the Flinders Ranges region responded by initiating long-wavelength (~150 km) flexing instabilities, localized by weaknesses and membrane stresses inherited from prior tectonic processes. This broad "flexing" produced a shallow, topographic high coincident with the current axis of the ranges, with flanking basins establishing their characteristic form floored by preneotectonic material which slopes away from the axis of the ranges. The onset of failure in the late Neogene reflects increases in stress levels forced principally by changes in the coupling between the Pacific and Australian plates. At this time, seismogenic strain began to accumulate in the upper crust, with localized failure reflecting spatial variations in lithospheric strength controlled by its thermal structure.

[50] **Acknowledgments.** Wolfgang Preiss is thanked for drawing our attention to the Burra Fault locality. Careful and insightful reviews by Jean-Phillipe Avouac and several anonymous reviewers are greatly appreciated.

References

Alley, N. F., and J. M. Lindsay (1995), Tertiary, in *The Geology of South Australia*, vol. 2, *The Phanerozoic*, edited by J. F. Drexel and W. V. Preiss, *Bull. S. Aust. Geol. Surv.*, *54*, 219–281.

Bassi, G. (1991), Factors controlling the style of continental rifting: Insights from numerical modeling, *Earth Planet. Sci. Lett.*, *105*, 430–452.

Belperio, A. P. (1995), Quaternary, in *The Geology of South Australia*, vol. 2, *The Phanerozoic*, edited by J. F. Drexel and W. V. Preiss, *Bull. S. Aust. Geol. Surv.*, *54*, 219–281.

Brace, W. F., and D. L. Kohlstedt (1980), Limits on lithospheric stress imposed by laboratory experiments, *J. Geophys. Res.*, *85*, 6248–6252.

Braun, J., and C. Beaumont (1987), Styles of continental rifting: results from dynamic models of lithospheric extension, in *Sedimentary Basins and Basin-Forming Mechanisms*, edited by C. Beaumont and A. J. Tankard, *Can. Soc. Pet. Geol. Mem.*, *12*, 241–258.

Callen, R. A. (1974), Geology of the Frome 1:250,000 geological map and adjacent regions, Dep. of Mines S. Aust., Adelaide.

Callen, R. A., and R. H. Tedford (1976), New Late Cainozoic rock units and depositional environments, Lake Frome area, South Australia, *Trans. R. Soc. S. Aust.*, *100*, 125–167.

Clark, D., and M. Leonard (2003), Principal stress orientations from multiple focal-plane: New insights into the Australian intraplate stress field, in *Evolution and Dynamics of the Australian Plate*, edited by R. R. Hillis and D. Muller, *Spec. Publ. Geol. Soc. Aust.*, *22*, 91–105.

Cloetingh, S., and R. Wortel (1986), Stress in the Indo-Australian Plate, *Tectonophysics*, *132*, 49–67.

Cloetingh, S., E. Burov, and A. Poliakov (1999), Lithosphere folding: Primary response to compression? (from central Asia to Paris basin), *Tectonics*, *18*, 1064–1083.

Coats, R. P., and A. H. Blissett (1971), The regional and economic geology of the Mount Painter province, report, Adelaide Dep. of Mines, Adelaide, Australia, S., Australia.

Coblentz, D., M. Sandiford, R. Richardson, S. Zhou, and R. Hillis (1995), The origins of the Australian stress field, *Earth Planet. Sci. Lett.*, *133*, 299–309.

Coblentz, D., S. Zhou, R. Hillis, R. Richardson, and M. Sandiford (1998), Topography, plate-boundary forces and the Indo-Australian intraplate stress field, *J. Geophys. Res.*, *103*, 919–931.

Costain, J. K., G. A. Bollinger, and J. A. Speer (1987), Hydroseismicity—A hypothesis for the role of water in the generation of intraplate seismicity, *Geology*, *15*, 618–621.

Cull, J. P. (1982), An appraisal of Australian heat-flow data, *BMR J. Aust. Geol. Geophys.*, *7*, 11–21.

Ervin, C. P., and L. D. McGinnis (1975), Reelfoot rift: Reactivated precursor to the Mississippi embayment, *Geol. Soc. Am. Bull.*, *86*, 1287–1295.

Gaul, B. A., M. O. Michael-Leiba, and J. M. W. Rynn (1990), Probabilistic earthquake risk maps of Australia, *Aust. J. Earth Sci.*, *37*, 169–187.

Geller, C. A., J. K. Weissel, and R. N. Anderson (1983), Heat transfer and intraplate deformation in the central Indian Ocean, *J. Geophys. Res.*, *88*, 1018–1032.

Gerbault, M. (2000), At what stress level is the central Indian ocean buckling?, *Earth Planet. Sci. Lett.*, *178*, 165–181.

Gerbault, M., S. Henrys, and F. Davey (2003), Numerical models of lithospheric deformation forming the Southern Alps of New Zealand, *J. Geophys. Res.*, *108*(87), 2341, doi:10.1029/2001JB001716.

Gibson, H. J., and K. Stuwe (2000), Multiphase cooling and exhumation of the southern Adelaide Fold Belt: constraints from apatite fission track data, *Basin Res.*, *12*, 31–45.

Greenhalgh, S. A. L., D. Malps, and K. McDougall (1994), South Australian earthquakes, *Aust. J. Earth Sci.*, *41*, 483–495.

Gutenberg, B., and C. F. Richter (1944), Earthquake study in southern California, *Eos Trans. AGU*, *26*, 313–314.

Hanks, T. C., and H. Kanamori (1979), Fault mechanics, *J. Geophys. Res.*, *84*, 2145.

Hansen, D. L., and S. B. Nielsen (2002), Does thermal weakening explain basin inversion? Stochastic modelling of the thermal structure beneath sedimentary basins, *Earth Planet. Sci. Lett.*, *198*, 113–127.

Hansen, D. L., and S. B. Nielsen (2003), Why rifts invert in compression, *Tectonophysics*, *373*, 5–24.

Herrmann, R. B., and J.-A. Canas (1978), Focal mechanism studies in the New Madrid Seismic Zone, *Bull. Seismol. Soc. Am.*, *68*, 1095–1102.

Hillis, R. P., J. J. Meyer, and D. D. Reynolds (1998), The Australian stress map, *Explor. Geophys.*, *29*, 420–427.

Houseman, G. A., J. P. Cull, P. M. Muir, and H. L. Paterson (1989), Geothermal signatures of uranium ore deposits on the Stuart Shelf of South Australia, *Geophysics*, *54*, 158–170.

Jaeger, J. C., and N. G. W. Cook (1969), *Fundamentals of Rock Mechanics*, CRC Press, Boca Raton, Fla.

Johnston, A. C. (1994a), The stable continental region earthquake database, in The earthquakes of stable continental regions, 1, Assessment of large earthquake potential. In The earthquakes of stable continental regions, *Rep. TR-102261-1*, pp. 3-1–3-80, Electr. Power Res. Inst., Palo Alto, Calif.

Johnston, A. C. (1994b), Seismotectonic interpretations and conclusions from the stable continental region seismicity database, in *The Earthquakes of Stable Continental Regions*, *Rep. TR-102261*-1, pp. 4-1–4-102, Electr. Power Res. Inst., Palo Alto, Calif.

Johnston, A. C. (1996), Seismic moment assessment of earthquakes in stable continental regions-II, Historical seismicity, *Geophys. J. Int.*, *125*, 639–678.

Johnston, A. C., and L. R. Kanter (1990), Earthquakes in stable continental crust, *Sci. Am.*, *262*(3), 68–75.

Johnston, A. C., and E. S. Schweig (1996), The enigma of the New Madrid earthquakes of 1811–1812, *Annu. Rev. Earth Planet. Sci.*, *24*, 339–384.

Karner, G. D. (1986), Effects of lithospheric in-plane stress on sedimentary basin stratigraphy, *Tectonics*, *5*, 573–588.

Karner, G. D., N. W. Driscoll, and J. K. Weissel (1993), Response of the lithosphere to in-plane force variations, *Earth Planet. Sci. Lett.*, *114*, 397–416.

Kostrov, V. V. (1974), Seismic moment and energy of earthquakes, and seismic flow of rock, *Phys. Solid Earth*, *1*, 13–21.

Lambeck, K. (1983), The role of compressive forces in intracratonic basin formation and mid-plate orogenies, *Geophys. Res. Lett.*, *10*, 845–848.

Martinod, J., and P. Molnar (1995), Lithospheric folding in the Indian Ocean and the rheology of the oceanic plate, *Bull. Soc. Geol. Fr.*, *166*, 813–821.

McLaren, S., W. J. Dunlap, M. Sandiford, and I. McDougall (2002), Thermochronology of high heat-producing crust at Mount Painter, South Australia: Implications for tectonic reactivation of continental interiors, *Tectonics*, *21*(4), 1020, doi:10.1029/2000TC001275.

McLaren, S., M. Sandiford, M. Hand, N. Neumann, L. Wyborn, and I. Bastrakova (2003), The hot southern continent: Heat flow and heat production in Australian Proterozoic terranes, in *Evolution and Dynamics of the Australian Plate*, edited by R. R. Hillis and D. Muller, *Spec. Publ. Geol. Soc. Aust.*, *22*, 151–161.

Minster, J. B., and T. H. Jordan (1978), Present-day plate motion, *J. Geophys. Res.*, *83*, 5331–5334.

Molnar, P. (1989), Brace-Goetze strength profiles, the partitioning of strike-slip and thrust faulting at zones of oblique convergence and the stress-heat flow paradox of the San Andreas Fault, in *Fault Mechanics and Transport Properties of Rocks*, edited by B. Evans and T.-F. Wong, pp. 435–460, Elsevier, New York.

Neumann, N., M. Sandiford, and J. Foden (2000), Regional geochemistry and continental heat flow: implications for the origin of the South Australian heat flow anomaly, *Earth Planet. Sci. Lett.*, *183*, 107–120.

Nielsen, S. B., and D. L. Hansen (2000), Physical explanation of the formation and evolution of inversion zones and marginal basins, *Geology*, *28*, 875–878.

Paul, E., T. Flottmann, and M. Sandiford (1999), Structural geometry and controls on basement-involved deformation in the northern Flinders Ranges, Adelaide Fold Belt, South Australia, *Aust. J. Earth Sci.*, *46*, 343–354.

Preiss, W. V. (1987), The Adelaide geosyncline: Late Proterozoic stratigraphy, sedimentation, palaeontology and tectonics, *Geol. Soc. S. Aust. Bull.*, *53*, 29–34.

Quigley, M. C., M. Cupper, and M. Sandiford (2005), Quaternary faults of south central Australia: palaeoseismicity, slip rates and origin, *Aust. J. Earth Sci.*, in press.

Ranalli, G. (1995), *Rheology of the Earth*, 413 pp., CRC Press, Boca Raton, Fla.

Reynolds, S. D., R. R. Hillis, and D. D. Coblentz (2002), The Australian stress field: Implications for plate boundary forces, paper presented at Geoscience 2002: Expanding Horizons, 16th Australian Geological Convention, Geol. Soc. of Aust., Melbourne.

Richardson, R. M. (1987), Modelling the tectonics of the Indo-Australian plate (abstract), *Eos Trans. AGU*, *68*, 1466.

Sandiford, M. (1999), Mechanics of basin inversion, *Tectonophysics*, *305*, 109–120.

Sandiford, M. (2003), Neotectonics of southeastern Australia: Linking the Quaternary faulting record with seismicity and in situ stress, in *Evolution and Dynamics of the Australian Plate*, edited by R. R. Hillis and D. Muller, *Spec. Publ. Geol. Soc. Aust.*, *22*, 101–113.

Sandiford, M., and S. McLaren (2002), Tectonic feedback and the ordering of heat producing elements within the continental lithosphere, *Earth Planet. Sci. Lett.*, *204*, 133–150.

Sandiford, M., D. Coblentz, and R. M. Richardson (1995), Focusing ridge-torques during continental collision in the Indo-Australian plate, *Geology*, *23*, 653–656.

Sandiford, M., E. Paul, and T. Flottmann (1998), Sedimentary thickness variations and deformation intensity during basin inversion in the Flinders Ranges, South Australia, *J. Struct. Geol.*, *20*, 1721–1731.

Sandiford, M., M. Leonard, and D. Coblentz (2003), Geological constraints on active seismicity in southeast Australia, in *Earthquake Risk Mitigation*, edited by C. J. L. Wilson, N. K. Lam, and G. Gibson, pp. 1–10, Aust. Earthquake Eng. Soc., Melbourne.

Sandiford, M., N. Wallace, and D. Coblentz (2004), Origin of the in situ stress field in southeastern Australia, *Basin Res.*, *16*, 325–338.

Sandiford, M., D. Coblentz, and W. P. Schellart (2005), Evaluating slab-plate coupling in the Indo-Australian plate, *Geology*, *33*, 113–116.

Simons, F. J., M. T. Zuber, and J. Korenaga (2000), Isostatic response of the Australian lithosphere: Estimation of the effective elastic thickness and anisotropy using multitaper spectral analysis, *J. Geophys. Res.*, *105*, 19,163–19,184.

Sonder, L., and P. England (1986), Vertical averages of rheology of the continental lithosphere; relation to thin sheet parameters, *Earth Planet. Sci. Lett.*, *77*, 81–90.

Spassov, E., and B. L. N. Kennett (2000), Stress and faulting in south east Australia as derived from the

strongest earthquakes in the region, *J. Asian Earth Sci.*, *18*, 17–23.

Sprigg, R. C. (1946), Reconnaissance geological survey of portion of the western escarpment of the Mount Lofty ranges, *Trans. R. Soc. S. Aust.*, *70*, Part 2, 313–347.

Stephenson, R. A., and S. Cloetingh (1991), Some examples and mechanical aspects of continental lithospheric folding, *Tectonophysics*, *188*, 27–37.

Sykes, L. R. (1978), Intraplate seismicity, reactivation of pre-existing zones of weakness, alkaline magmatism and other tectonism post-dating continental fragmentation, *Rev. Geophys.*, *16*, 621–688.

Thomson, B. P. (1969), The Kanmantoo Group and Early Palaeozoic tectonics, in *Handbook of South Australian Geology*, edited by L. W. Parkin, pp. 97–108, Geol. Surv. of S. Aust., Adelaide.

Veevers, J. J., and P. J. Conaghan (1984), *Phanerozoic Earth History of Australia*, 418 pp., Oxford Univ. Press, New York.

Weissel, J. K., R. N. Anderson, and C. A. Geller (1980), Deformation of the Indo-Australian Plate, *Nature*, *287*, 284–291.

Wellman, P., and S. A. Greenhalgh (1988), Flinders/Mount Lofty Ranges, South Australia their uplift, erosion, and relationship to crustal structure, *Trans. R. Soc. S. Aust.*, *112*, 11–19.

Wesnousky, S. G. (1980), The craton: Its effect on the distribution of seismicity and stress in North America, *Earth Planet. Sci. Lett.*, *48*, 348–355.

Williams, G. E. (1973), Late Quaternary piedmont sedimentation, soil formation and paleoclimates in arid South Australia, *Z. Geomorph.*, *17*, 102–125.

Zuber, M. T., T. D. Bechtel, and D. W. Forsyth (1989), Effective elastic thicknesses of the lithosphere and mechanisms of isostatic compensation in Australia, *J. Geophys. Res.*, *94*, 9353–9367.

J. Célérier, Research School of Earth Sciences, Australian National University, Mills Road, Canberra 0200, Australia. (julien.celerier@anu.edu.au)

D. L. Hansen, Department of Earth Sciences, University of Aarhus, Finlandsgade 6-8, DK-8200 Aarhus N, Denmark.

M. Quigley and M. Sandiford, School of Earth Sciences, University of Melbourne, Melbourne, Victoria, 3010, Australia.

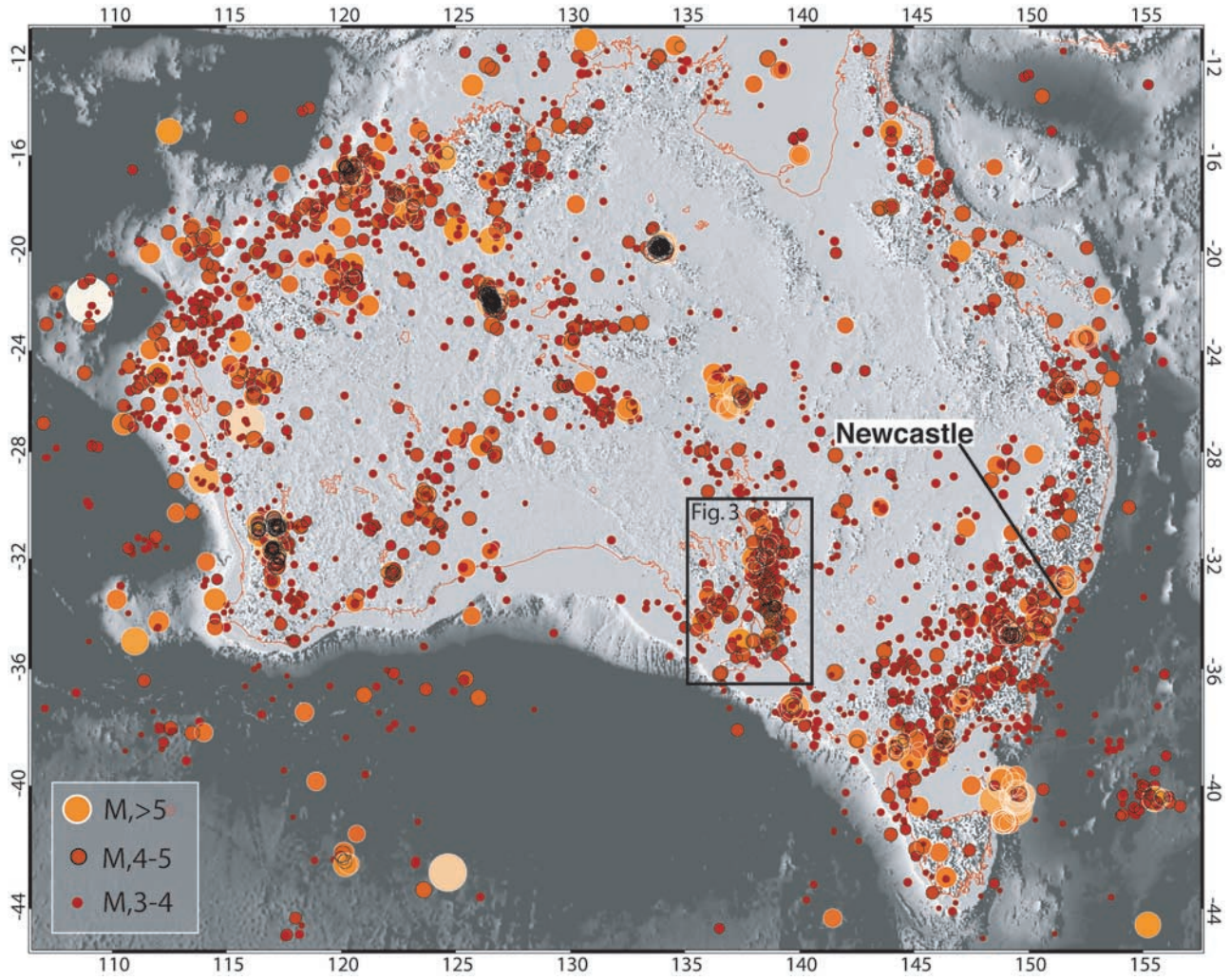

Figure 1. Distribution of Australian seismicity ($M > 3$). Earthquake epicenter data are courtesy of Geoscience Australia. Magnitude measures are based on local magnitudes (M_L) for $M < 5.5$ and surface magnitude (M_s) for $M > 5.5$.

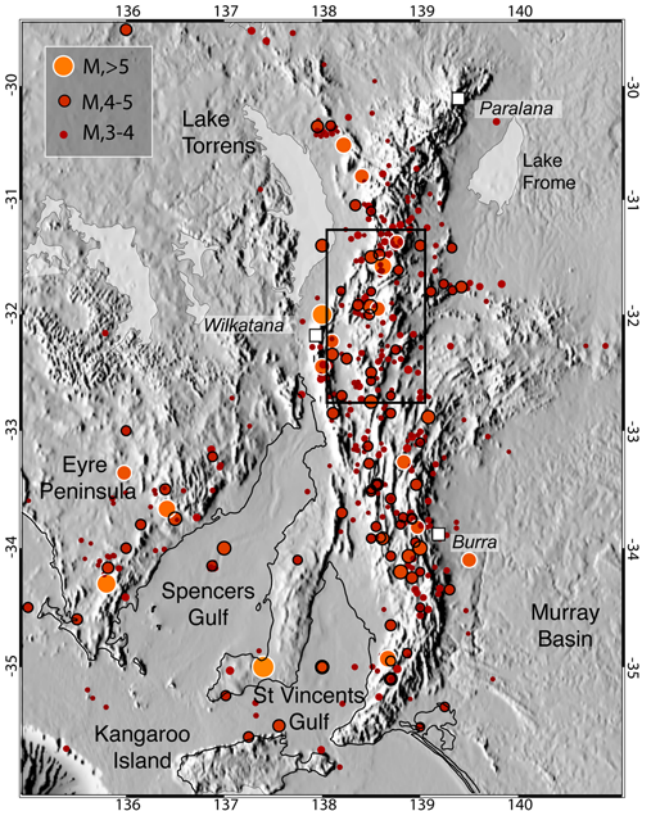

Figure 3. Seismicity pattern of South Australia showing the upland system of the Flinders and Mount Lofty ranges. The Mount Lofty Ranges refer to the southern part of this upland system (south of 34°S), while the Flinders Ranges refer to region north of about 33°30S. Note the anomalously low depressions flanking the ranges (see Figure 4). Around the Flinders Ranges these depressions form internally draining playa lake systems. Earthquake epicenter data are courtesy of Geoscience Australia. Rectangular region shows the region of seismicity used to define Guttenberg-Richter characteristics in Figure 2. Magnitude measures are based on local magnitudes (M_L) for $M < 5.5$ and surface magnitude (M_s) for $M > 5.5$.